Journal of Hazardous Materials 163 (2009) 98–108

Contents lists available at ScienceDirect

Journal of Hazardous Materials

journal homepage: www.elsevier.com/locate/jhazmat

Adsorptive features of polyacrylamide–apatite composite for Pb^{2+}, UO_2^{2+} and Th^{4+}

Ulvi Ulusoy*, Recep Akkaya

Cumhuriyet University, Department of Chemistry, Sivas 58140, Turkey

ARTICLE INFO

Article history:
Received 30 October 2007
Received in revised form 18 June 2008
Accepted 18 June 2008
Available online 26 June 2008

Keywords:
Adsorption
Hydroxyapatite
Composite
Metal
Polyacrylamide

ABSTRACT

Micro-composite of polyacrylamide (PAA) and apatite (Apt) was prepared by direct polymerization of acrylamide in a suspension of Apt and characterized by means of FT-IR, XRD, SEM and BET analysis. The adsorptive features of PAA–Apt and Apt were then investigated for Pb^{2+}, UO_2^{2+} and Th^{4+} in view of dependency on ion concentration, temperature, kinetics, ion selectivity and reusability. Experimentally obtained isotherms were evaluated with reference to Langmuir, Freundlich and Dubinin–Radushkevich (DR) models. Apt in PAA–Apt had higher adsorption capacity (0.81, 1.27 and 0.69 mol kg^{-1}) than bare Apt (0.28, 0.41 and 1.33 mol kg^{-1}) for Pb^{2+} and Th^{4+}, but not for UO_2^{2+}. The affinity to PAA–Apt increased for Pb^{2+} and UO_2^{2+} but not changed for Th^{4+}. The values of enthalpy and entropy changed were positive for all ions for both Apt and PAA–Apt. Free enthalpy change was $\Delta G < 0$. Well compatibility of adsorption kinetics to the pseudo-second-order model predicated that the rate-controlling step was a chemical sorption. This was consistent with the free energy values derived from DR model. The reusability tests for Pb^{2+} for five uses proved that the composite was reusable to provide a mean adsorption of $53.2 \pm 0.7\%$ from 4×10^{-3} M Pb^{2+} solution and complete recovery of the adsorbed ion was possible ($98 \pm 1\%$). The results of this investigation suggested that the use of Apt in the micro-composite form with PAA significantly enhanced the adsorptive features of Apt.

1. Introduction

The adsorption procedures are introduced as a favorable way for the remediation of aquatic waste because of its efficacy, practicality and economical feasibility, as depending on the used adsorbents.

Polymers have attracted great interest because they are easily and effectively produced in a wide variety of compositions, and exhibit specific sorption properties after modification with various functional groups. For instance, poly(1,8-di-aminonaphthalene) microparticles was the sorbent for removal and recovery of Ag^+ ions with the highest adsorptivity of Ag^+ ions of 1924 mg g^{-1} [1]. High sorption capacities with very rapid uptake by poly(*p*-phenylenediamine) and poly(*m*-phenylenediamine) with strong chemoresistance have been reported for lead ions [2,3]. Despite the fact that the considerable successes obtained from such studies with synthetic polymers, the high cost has remained controversial.

The low cost adsorbents are the naturally occurring materials with high abundance such as aluminosilicates; clay and zeolite [4]. Apatitic minerals have also been considered amongst ideal low cost adsorbents because of their high sorption capacity for metal ions, the least solubility and the highest stability in a wide range of pH, and high stability under reducing/oxidizing conditions [5]. Hydroxyapatite [$Ca_{10}(PO_4)_6(OH)_2$] as an apatitic mineral is the main calcium phosphate component of bone. It can be produced by mining mineral deposits [6], from calcinations of bone [7] or through precipitation from calcium phosphate solutions [8].

Due to their suitable features, apatitic minerals, hydroxyapatite in particular has been the scope of considerable number of adsorption investigations. For example, adsorptive features of Ca–hydroxyapatite in view of the influence of sorption protocol, kinetics and diffusion were investigated for Cd^{2+} [9,10], UO_2^{2+} [5,11], Pu^{6+} [12] and Co^{2+} [13] in aqueous solutions. The ion-exchange features of Ba–hydroxyapatite for Cu^{2+}, Pb^{2+}, Zn^{2+}, Cd^{2+} and Co^{2+}, and the enhancement of Ba^{2+} exchangeability with Pb^{2+} were of interest in studies performed by Sugiyama et al. [14,15]. Sorption properties of natural and synthetic carbonate fluoroapatites were compared by Perrone et al. [16] for Ni^{2+}. The natural form of hydroxyapatite were used in removal of Cu^{2+}, $Cd^{2+}$and Pb^{2+} by Mavropoulos et al. [6] and Sarioglu et al. [17]. Recent investigations on this topic have also focused on surface modifications to provide a wider applicability of these minerals from adsorption studies to medical applications [18–21]. In consequence, all above-mentioned studies coherently show the advantages of apatitic minerals (with or without modifications) in removal of metal ions.

* Corresponding author. Tel.: +90 346 2191010x1623; fax: +90 346 2191186.
E-mail address: ulusoy@cumhuriyet.edu.tr (U. Ulusoy).

0304-3894/$ – see front matter © 2008 Elsevier B.V. All rights reserved.
doi:10.1016/j.jhazmat.2008.06.064

Further researches require enhancing adsorption capacity and practical usage of apatitic minerals, since the aggregation and coagulation of mineral particles under varying conditions of temperature and electrolytes lead variations in flow properties of these minerals. This is an undesired feature for their practical use as adsorbents since it may result in e.g. hydrodynamic constraints in chromatographic and/or column applications. The use of the mineral as its composite with a polymer may be helpful to overcome these limitations. Beside its practicality, the composition may display more properties of an effective adsorbent than the bare mineral. The polymer should be capable of swelling in aquatic solutions, enabling the diffusion and/or transfer of ions towards adsorption sites of the embodied mineral and should be inert for metal ions. As a hydrogel polymer, the cross-linked polyacryamide (PAA) should provide these requirements as it was proved for bentonite and zeolite [22,23]. Such a composite, in which the mineral ground to the intended size dispersed as a mineral phase in a polymer (with guest and host resemblance) should be a phase separated micro-composites with reference to the classification by Alexandre and Dubois [24]. Because, hydroxyapatite does not have a layered structure like bentonite to provide intercalated or exfoliated nanocomposites [22,25].

The aim of this investigation was to introduce the composite of apatite (Apt) with PAA as a new material (PAA–Apt) for practical use of Apt in adsorption procedures. The preparation and characterization of PAA–Apt, and its comparative adsorptive features with bare Apt with reference to the dependency on concentrations and temperature, and the adsorption kinetics for Pb^{2+}, UO_2^{2+} and Th^{4+} were investigated. The metal cations represented the hazardousness in view of toxicity and radioactivity, different oxidation states and ionic compositions. Besides this, the recovery of such metals may also be economical interests. The adsorptive features were evaluated on the base of adsorption parameters derived from the compatibility of experimentally obtained adsorption isotherms to Langmuir, Freundlich and Dubinin–Radushkevich (DR) models. Additional considerations were also given to the ion selectivity and reusability of the composite for the studied ions.

2. Experimental

2.1. Reagents

Acrylamide monomer, *N,N′*-methylenebisacrylamid, *N,N,N′,N′*-tetramethylethylenediamine, $Pb(NO_3)_2$, $UO_2(NO_3)_2{\cdot}6H_2O$ and $Th(NO_3)_4{\cdot}4H_2O$ were purchased from Sigma Aldrich. Arsenazo III (disodium salt) was obtained from Acros. Merck was the supplier of 4-(2′-pyridylazo)-resorcinol (PAR). All chemicals used were of analytical reagent grade.

Samsun Fertilizer Laboratories (Turkey) supplied the phosphate rock as it was ground and sieved in the size of 100 mesh. The composition of the rock was 49.08% of CaO, 30.97% of P_2O_5, 3.21% of SiO_2, 3.63% of F, 5.14% of CO_2, 2.86% of SO_3, 1.14% of M_2O_3 (Fe + Al) and 0.68% of MgO [14] in comparison to a pure phosphate rock with an empirical formulae of $Ca_5(PO_4)_3(OH)_{0.3333}F_{0.3333}Cl_{0.3333}$ composed of 55.1% of CaO and 41.8% of P_2O_5 (http://webmineral.com/data/Apatite.shtml). Both pure phosphate rock and hydroxyapatite synthetically obtained with the chemical reaction between $Ca(OH)_2$ and H_3PO_4 have a stoichiometric ratio of $mol_{Ca}/mol_P \approx 1.65$ [8]. However, the ratio values for phosphate rocks given in the literature is different from this value, as reported by Mavropoulos et al. [6], where the mean of ratios with ±S.E.M. for 10 different rocks was 2.21 ± 0.31. The studied rock had a ratio of 2.01, the closeness of this value to those given in the literature should be a supportive evidence for the apatite composition of the rock.

All experiments were always performed in duplicates. ±5% was the limit of experimental error of each duplicates, any experiment resulted in higher than this limit was repeated. Time to attain equilibration between solution and adsorbent was chosen as 24 h, as appropriate to the convention, despite the fact that the studies related to kinetics implied a shorter time than this duration (see below).

2.2. Preparation and characterization of PAA–Apt composite

For preparation of 3 g of PAA–Apt, 1 g of Apt in 20 mL of water was stirred 15 min to obtain a homogeneous suspension. 10 mL of solution containing 2 g of acrylamide monomer to provide a mass ratio 2:1 was added to the suspension and stirred additional 5 min. 0.2 g of *N,N′*-methylenebisacrylamid and 50 mg ammoniumpersulphate dissolved in 10 mL distilled water was contained on to the suspension. Finally, 100 μL of *N,N,N′,N′*-tetramethylethylenediamine was added to propagate the polymerization at 25 °C [26]. PAA–Apt gel was washed after completion of the polymerization with distilled water until the effluent attained neutral pH. The gel was dried at ambient temperature, ground and sieved to a particle −20 mesh size, and stored in polypropylene container. To avoid the variations in characteristics dependent on the preparation, A 50 g lot of PAA–Apt was prepared to conduct the overall investigation. Bare PAA was also prepared for comparison of structural and swelling features of the composite and Apt with PAA. 0.1 g of dried samples were weighed and let to swell in tubes for the equilibrium with water, the swollen samples were then weighed to find swelling ratio as percentage with reference to the dry weights.

FT-IR (Mattson 1000, UK) was employed to characterize the chemical structure of Apt and PAA–Apt. XRD (Rigaku Dmax 2200, using Cu Kα radiation, a proportional counter, 2θ/min scan rate) in Department of Physics (Hacettepe University/Turkey) was used for powder diffractions of bare Apt and PAA–Apt. Adsorption surface area (BET by the use of N_2 sorption system, Quantachrome Instruments) measurements and scanning electron microscopy (SEM; JEOL/JSM-6335F) analysis were performed in Tubitak/Gebze (Turkey) Laboratories.

2.3. Pb^{2+}, UO_2^{2+} and Th^{4+} adsorption

Adsorptive features of the Apt and PAA–Apt were investigated for Pb^{2+}, UO_2^{2+} and Th^{4+}. 0.1 g of Apt and PAA–Apt in the studied solutions was equilibrated with 10 mL of Pb^{2+}, UO_2^{2+} and Th^{4+} at concentrations within the range from 1×10^{-4} to 8×10^{-3} mol L^{-1} (25–2000 mg L^{-1}). The adsorbent-solution systems were equilibrated for 24 h at 298 K in a thermostatic water bath and the suspensions were then centrifuged at 2500 rpm for 3 min. The initial and final pH values of the solutions were always within the range of 3–5.

The adsorption dependence on pH was tested for each ion for 5 pH values (1–5 with 1 interval); 0.1 g of Apt or PAA–Apt was added in solutions adjusted to the desired pH, containing 5×10^{-4} mol L^{-1} of ions. Mass dependency of the adsorption was also checked for PAA–Apt; 25, 50, 75 and 100 mg of the composite were interacted with solutions of the ions at 5×10^{-3} mol L^{-1}. The adsorbed amounts were determined by analyzing of the supernatants obtained after the procedure given above.

PAR was used as complex forming reagent for determination of Pb^{2+} in the supernatants [23]. A solution of 3.5×10^{-3} mol L^{-1} of PAR in 0.7 mol L^{-1} of Tris–HCl at pH 8–9 was prepared. A 50 μL fraction of supernatant was added onto 3 mL of the reagent and the absorbance of the formed metal complex was measured at 510 nm. Arsenazo III was used as the dying reagent in determination of

UO_2^{2+} and Th^{4+} [27,28]. The solutions containing 0.04% Arsenazo III in HCl to provide pH 1.5 for UO_2^{2+} and in 2 mol L^{-1} $HClO_4$ for Th^{4+} analysis were prepared. A 50 μL fraction of supernatant was added onto 3 mL of the reagent and the absorbance was measured at 650 nm (Shimadzu-160A, Japan).

To confirm accuracy of the results obtained from the metal-dye detection, UO_2^{2+} and Pb^{2+} in some selected samples were also determined by radioactivity measurements by means of a gamma spectrometer [NaI(Tl) detector combined with a EG&G ORTEC multi-channel analyzer and software, MAESTRO 32, MCA Emulator, USA]. ^{212}Pb at secular equilibrium with ^{232}Th isolated from Th was used as isotopic tracer to monitor Pb^{2+} adsorption. The activity measured at 186 keV of ^{235}U at natural level in uranium composition and that at 238.6 keV of ^{212}Pb.

2.4. Temperature dependence of Pb^{2+}, UO_2^{2+} and Th^{4+} adsorption

Temperature effect on adsorption for determination of thermodynamic parameters was studied for three temperatures: 283, 298 and 313 K. Apt and PAA–Apt (0.1 g each) were equilibrated with solutions of Pb^{2+}, UO_2^{2+} and Th^{4+} at 3×10^{-3} mol L^{-1} at the chosen temperatures for 24 h. The samples were subjected to the same procedure described above; equilibrium concentrations and adsorbed amounts were then determined.

2.5. Adsorption kinetics

Ten milliliters of solution of each ion was added on to 0.1 g of Apt and PAA–Apt. 50 μL fractions of solution were withdrawn for 4 h, starting immediately after the solution-solid contact and continued with time intervals. Pb^{2+}, UO_2^{2+} and Th^{4+} contents of the fractions were determined.

2.6. Ion selectivity and reusability

The ion selectivity of Apt and PAA–Apt from solutions containing possible combinations of studied ions at equivalent concentrations (5×10^{-3} mol L^{-1}) was studied. Ten milliliters fraction of solutions containing the ions at possible combinations were poured on 0.1 g of Apt and PAA–Apt, the ion contents of equilibrium (after 24 h) solutions were measured. Neither Th^{4+} and Pb^{2+} nor UO_2^{2+} had any interference with each other when Th^{4+} was determined with Arsenazo III in 2 mol L^{-1} of $HClO_4$ [27,28]. The gamma spectrometric method was employed for determination of Pb^{2+} and UO_2^{2+}.

Hydrochloric acid at 1 mol L^{-1} is known as an effective regenerator for resins [29]; this effluent was also tested for the studied materials for Pb^{2+}. Five duplicates of 0.1 g Apt and PAA–Apt in polypropylene tubes were equilibrated with 10 mL of 4×10^{-3} mol L^{-1} Pb^{2+} for 24 h and the adsorbed amounts were determined. The contents of columns were eluted with 15 mL of 1 mol L^{-1} HCl with a flow rate of 1 mL min^{-1}. The recovery of Pb^{2+} with HCl was determined. The columns were then reconditioned with distilled water until the effluents had a neutral pH. Each sample was subjected to the same procedure for 4 sequential times to provide 5 uses in total.

2.7. Data evaluation

The amounts of adsorption of the ions (Q, mol kg^{-1}) were calculated from $Q = [(C_i - C_e)V/w]$, where C_i and C_e are the initial and equilibrium concentrations (mol L^{-1}), w is the mass of adsorbent (kg) and V is the solution volume (L). The Langmuir and Freundlich models defined with $Q = (K_L X_L C_e)/(1 + K_L C_e)$ and $Q = X_F C_e^{1/\beta}$ fit to the isotherms experimentally obtained, where X_L is the monolayer sorption capacity (mol kg^{-1}), K_L is the adsorption equilibrium constant (L mol^{-1}) related to the adsorption energy. X_F and '$1/\beta$' are empirical Freundlich constants associated with the capacity and intensity of adsorption ($1/\beta$ represents the heterogeneity of the adsorptive surface). The isotherms were also evaluated with reference to Dubinin–Radushkevich (DR) model to find out the constant (K_{DR}, mol^2 KJ^{-2}) related to the sorption energy from $Q = X_{DR} e^{-K_{DR}\varepsilon^2}$ where X_{DR} is sorption capacity (mol kg^{-1}) and ε is Polanyi potential given with $\varepsilon = RT \ln(1 + 1/C_e)$ in which R and T represent the ideal gas constant (8.314 J mol^{-1} K^{-1}) and absolute temperature (298 K). Free energy change (E, J mol^{-1}) required to transfer one mole of ion from the infinity in the solution to the solid surface was then derived from $E = (-2K_{DR})^{-1/2}$.

The distribution coefficients (K_d) were derived from $K_d = Q/C_e$ for each temperature and $\ln K_d$ was depicted against $1/T$ to provide adsorption enthalpy (ΔH, J mol^{-1}) and entropy (ΔS, J mol^{-1} K^{-1}) from the slopes ($\Delta H/R$) and intercepts ($\Delta S/R$) of the depictions with reference to $\ln K_d = \Delta S/R - \Delta H/(RT)$. Having had ΔH and ΔS, ΔG values were calculated from $\Delta G = \Delta H - T\Delta S$.

Equations related to the pseudo-second-order kinetic and intra-particle diffusion were $t/Q_t = 1/(kQ_{Mod}^2) + t/Q_{Mod}$ and $Q_t = k_i t^{1/2}$ (Weber and Morris model) where Q_t and Q_{Mod} are the adsorbed amounts (mol kg^{-1}) at time t and equilibrium, k and k_i are the rate constants were applied to the results of kinetic studies to be able to envisage the controlling mechanism of the adsorption process. Initial adsorption rate (H) was also calculated from $H = kQ_{Mod}^2$ [30–32].

Since PAA is an inert polymer for adsorption of the studied ions and the results obtained from the study for mass dependence of adsorption proved that the adsorbed amounts were linearly proportional with the mass of adsorbent ($R^2 > 0.980$, $p < 0.05$, not figured) for all studied ions, the values of Q (the adsorbed amounts) so that the obtained parameters for all studied procedures were calculated with reference to the Apt content of adsorbents (0.1 g for bare Apt and 0.035 g for PAA–Apt) to be able to show the effect of the Apt usage in composite form on adsorption.

3. Results and discussion

3.1. Structural evaluation

The FT-IR spectra, XRD patterns and SEM photographs of the composite and its components were compared in Fig. 1.

Broad and sharp appearance at 3200–3600 cm^{-1} in the FT-IR spectra were of the bonded and free O-H stretches. PAA and PAA–Apt (a and c) had clear counters around 3200 and 1560 cm^{-1} of NH, 1680 cm^{-1} of C=O of amide and 2900 cm^{-1} of C–H [23]. The typical frequencies defined around 1100, 950, 600 and 550 were of PO_4 groups of Apt in b and c of the FT-IR spectra [16,17]. There was not any clear indication that PAA and Apt interacted in forming any bond.

The typical Apt reflections in the XRD patterns of Apt and PAA–Apt confirmed that the main composition of the rock sample was apatite (Fig. 1) Intense increase in the background of PAA–Apt was due to the amorphous contribution of PAA to Apt. The crystallites size was derived from Scherer's formula; $S = 0.9K_\alpha/(\text{FWHM} \cos\theta)$, where S is the crystallite size (nm), K_α is the wavelength of X-ray beam (0.15406 nm), FWHM is the full with at half maximum (rad) of the considered θ reflection angle (°) with reference to the Miller indices at [L_{002}] and [L_{300}]. The sizes for the corresponding indices were calculated to be 34 and 30 nm for bare Apt and 24 and 21 nm for Apt in PAA–Apt indicating that the polymerization somehow diminished the mineral particles, if it was not a result of peak broadening due to the amorphous contribution of PAA. This predicts that adsorption of ions should increase due to

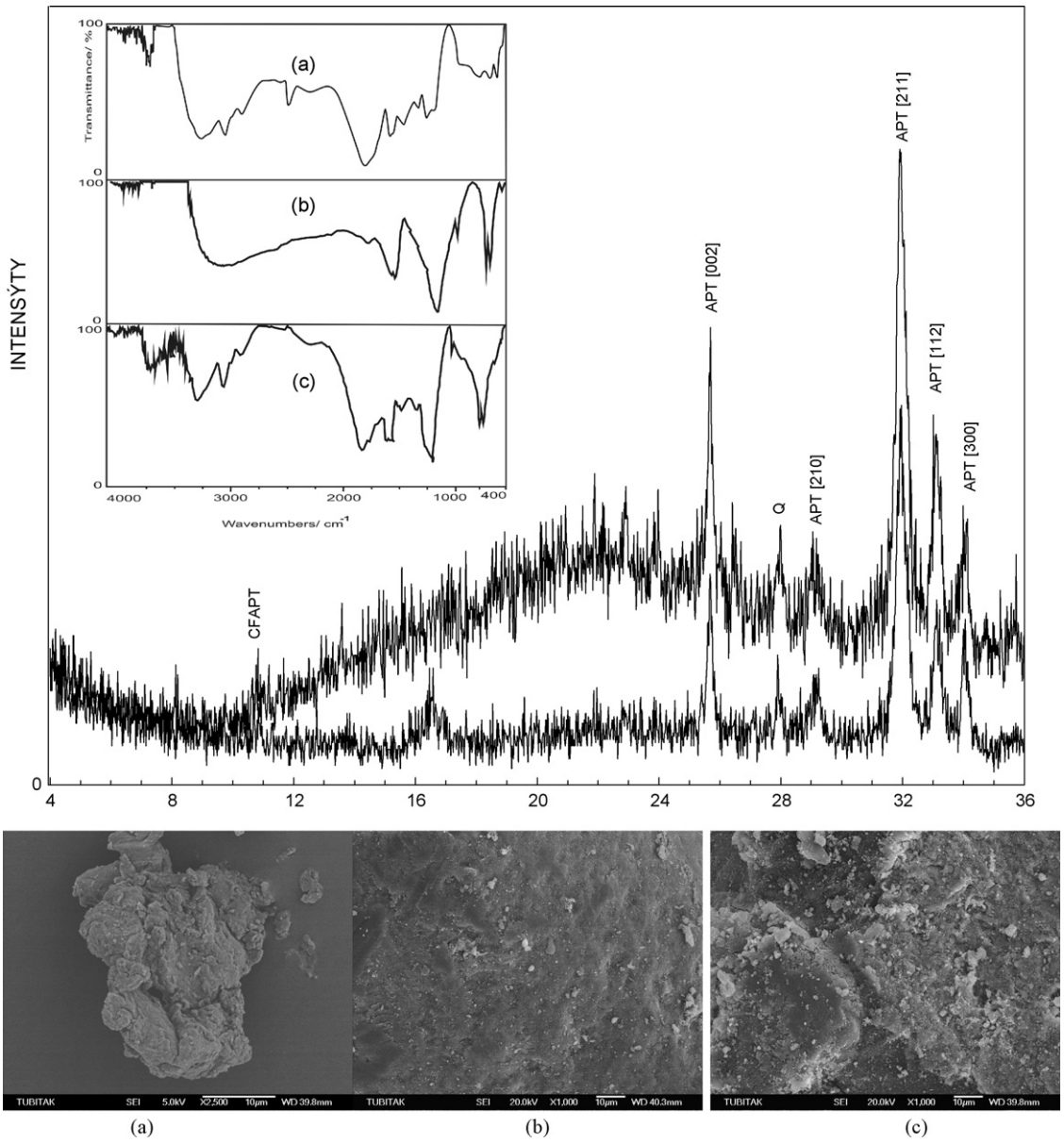

Fig. 1. The FT-IR spectra of PAA, Apt and PAA–Apt (a, b and c on the inside figure), XRD spectra of Apt (lower spectrum) and PAA–Apt [apatite (APT), carbonate fluoroapatite (CFA) and quartz (Q)] and SEM views of PAA, Apt and PAA–Apt (a–c).

the expansion of surface area to provide wider exposed sites for adsorption.

SEM views of the composite and its components were the evidence for the obvious change in PAA morphology by introduction of Apt. The morphology of PAA–Apt resembles a hybrid composition of its components. The dark colored textural appearances on PAA after Apt inclusion should be the impression of Apt crystallites (Fig. 1).

The BET values of studied materials were 17.4 and 8.3 $m^2\ g^{-1}$ for Apt and PAA–Apt. PAA like polymers have small BET surface areas, e.g. 0.25 and 2 $m^2\ g^{-1}$ [33,34], unless any specific procedure applied to obtain porosity. The results of this investigation indicated that Apt had a wider BET value than PAA–Apt, but the composite eventually gained a significant surface area (porosity) in comparison to PAA. This should also be considered as an advantage in favor of PAA–Apt in view of its adsorptive features.

Eventual consequence of the IR, XRD patterns, SEM views and BET results was homogeneous formation of the composite, i.e. the uniform dispersion of Apt in PAA.

The magnitude of swelling was found to be 120% for Apt, 1350% for PAA and 1400% for PAA–Apt. There was a slight increase for PAA–Apt in comparison to its individual components that might be attributed to the hydrophilic contribution of phosphate terminals of Apt in PAA–Apt to PAA.

3.2. Pb^{2+}, UO_2^{2+} and Th^{4+} adsorption

Experimentally attained adsorption isotherms and their compatibility to Langmuir, Freundlich and DR models of Pb^{2+}, UO_2^{2+} and Th^{4+} were provided in Fig. 2. The parameters derived from the models were introduced in Table 1.

The adsorption capacities (X_L, X_F and X_{DR}) obtained from the models were in the order of $UO_2^{2+} > Th^{4+} > Pb^{2+}$ for Apt and $Th^{4+} > Pb^{2+} > UO_2^{2+}$ for PAA–Apt. The sorption capacity of Apt in PAA significantly increased for Th^{4+} and Pb^{2+} but that drastically decreased for UO_2^{2+}.

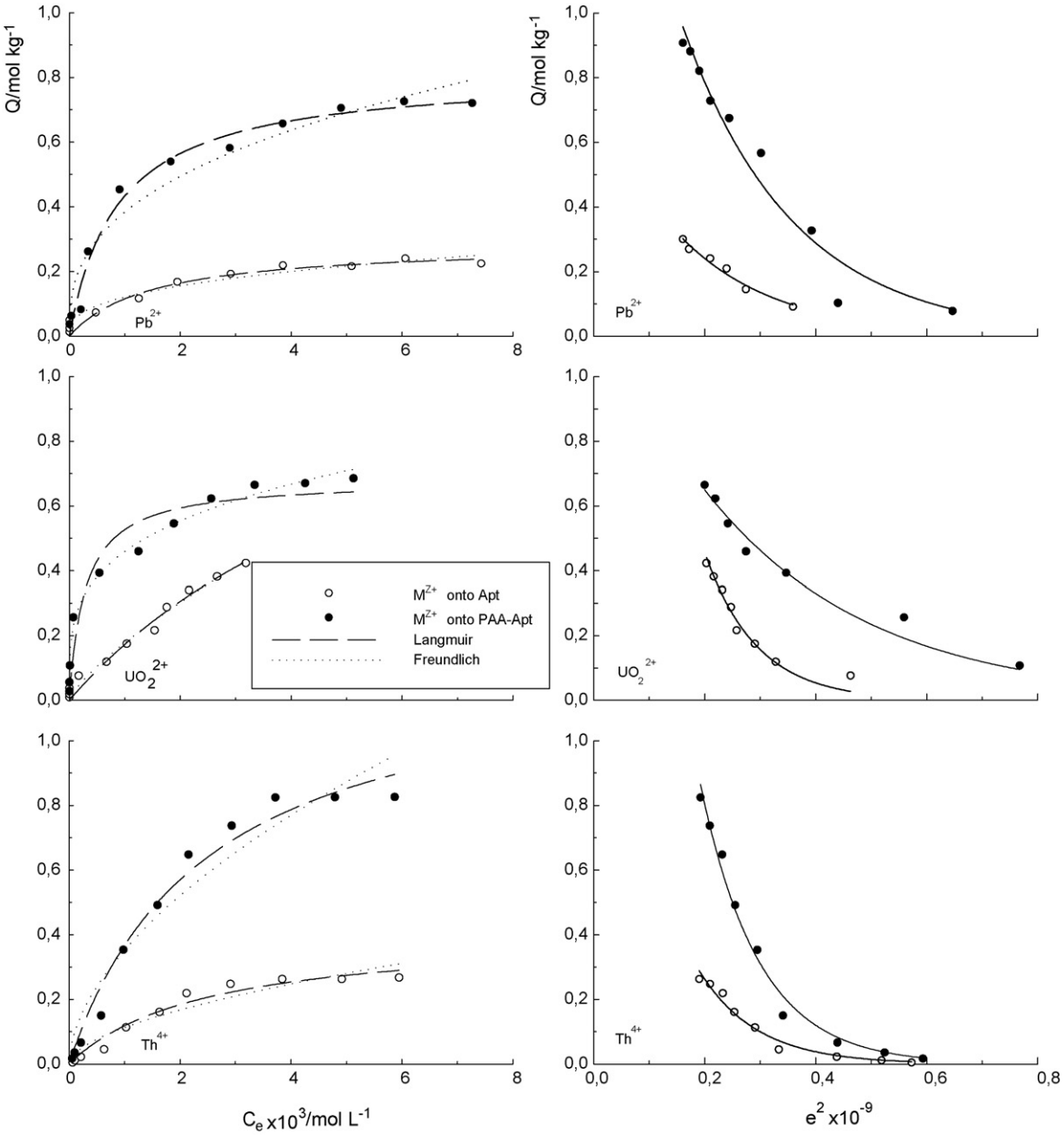

Fig. 2. Compatibility of experimentally obtained adsorption isotherms to Langmuir, Freundlich (Q vs. C_e) and DR (Q vs. ε^2) models.

Table 1
Langmuir, Freundlich and DR parameters for Pb^{2+}, UO_2^{2+} and Th^{4+} adsorption on to Apt and PAA–Apt

	Langmuir			Freundlich			DR		
	X_L (mol kg^{-1})	K_L (L mol^{-1})	R^2	X_F	β	R^2	X_{DR}	$-K_{DR} \times 10^9$ (mol^2 K J^{-2})	R^2
Pb^{2+}									
Apt	0.28	677	0.949	1.49	2.8	0.930	0.60	5.7	0.974
PAA–Apt	0.81	1142	0.983	4.82	2.7	0.949	1.71	5.0	0.961
UO_2^{2+}									
Apt	1.33	149	0.977	35.8	1.3	0.980	3.85	10.7	0.965
PAA–Apt	0.69	3440	0.936	2.95	3.7	0.985	1.28	3.4	0.971
Th^{4+}									
Apt	0.41	408	0.967	5.6	1.7	0.921	2.2	9.7	0.975
PAA–Apt	1.27	405	0.979	17.3	17.3	0.939	5.4	8.2	0.988

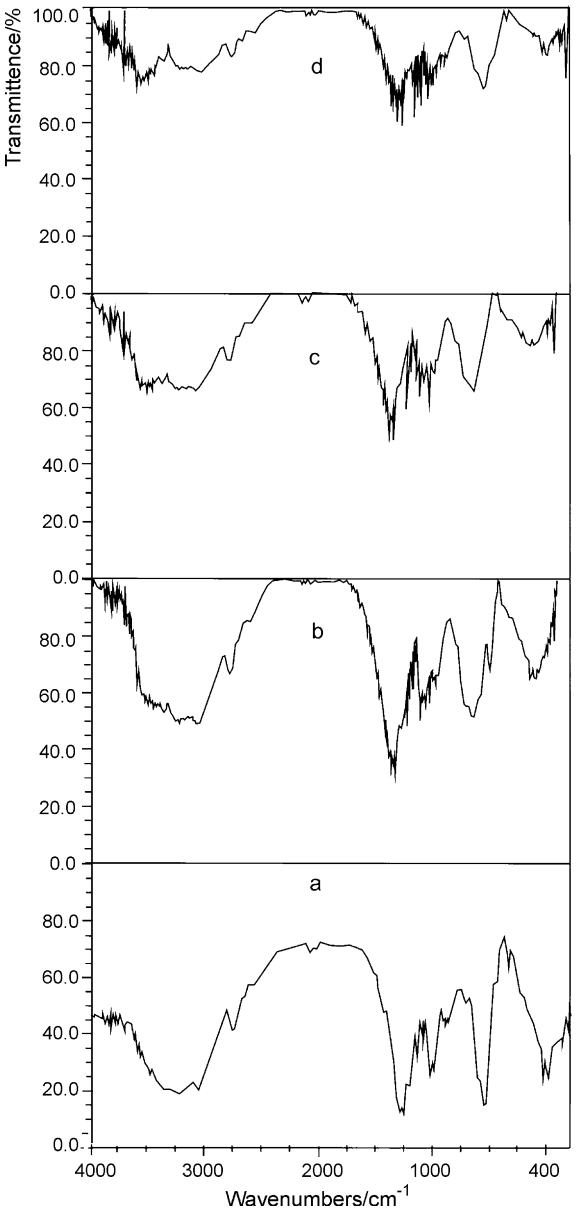

Fig. 3. The FT-IR spectra of pure PAA–Apt (a), UO_2^{2+} (b), Th^{4+} (c) and Pb^{2+} (d) adsorbed PAA–Apt.

The sequence of K_L and K_{DR} values, as a measure of the adsorption affinity was $Pb^{2+} > Th^{4+} > UO_2^{2+}$ for Apt and $UO_2^{2+} > Pb^{2+} > Th^{4+}$ for PAA–Apt in contrast to that of X and surface heterogeneity (β) values. Th^{4+} had the smallest K_L, but the highest X and β. This was contributed to the effective ionic charge (radii/ionic charge) which is in the sequence of UO_2^{2+} (253 pm/2) > Pb^{2+} (119 pm/2) > Th^{4+} (94 pm/4). The smaller has the higher mobility in the solution and in the hydrogel, for which the required energy for migration of ions towards the adsorbent and transference to the active sites to form complex with active terminals and/or to exchange of (possibly for Th^{4+} with Ca^{2+} with 100 pm/2 ionic charge) is expected to be lower than the others. However, the decline in sorption capacity for UO_2^{2+} with the highest ionic radius could be explained by the fact that sterical hindrance of PAA network in PAA–Apt. The FT-IR spectra of the pure and ions adsorbed PAA–Apt were compared in Fig. 3(a–d). There were distinguishable shrinks in all counters of pure PAA–Apt after ion sorption. This was explained by the fact that the formation of complex between ions and the active sites (mainly phosphate terminals) that resulted in increasing in transmittance, i.e. the decreasing sorption of IR radiation. Furthermore, the slight shifts and deformation in the peaks associated with PO_4 groups in Apt were of evidences for the complex formations.

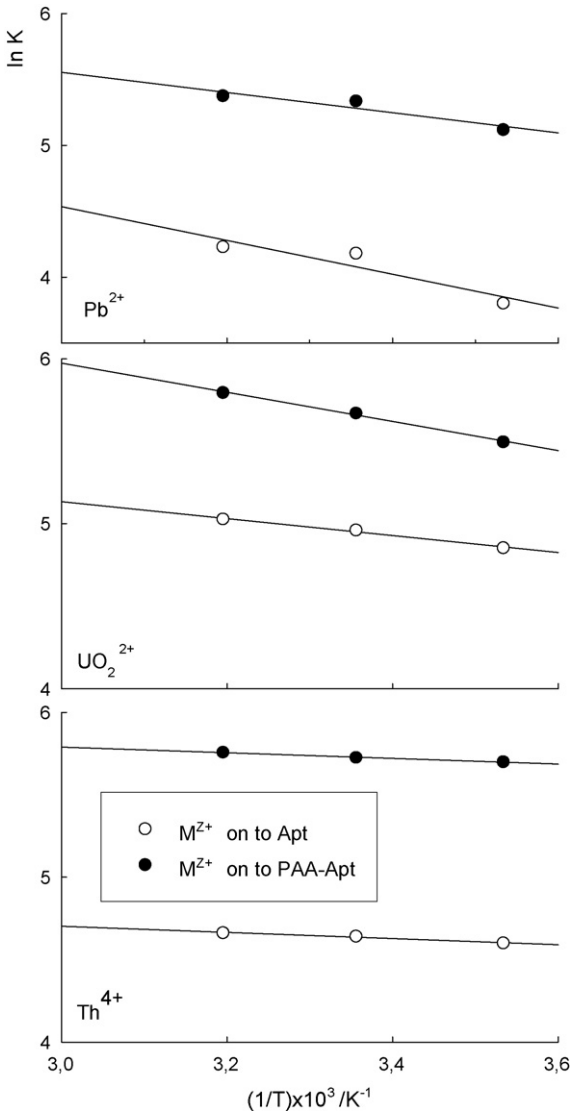

Fig. 4. Temperature dependence of the adsorption.

Any of the adsorption models, e.g. Langmuir can be used to predict the design of single-stage batch adsorption systems [35]. For reducing of an ion concentration from initial C_i (mol L^{-1}) to the desired level (C_e); the amounts of adsorbent, W (kg) required to add in a volume of solution, V (L) can be calculated from $W/V = (C_i - C_e)/(K_L X_L C_e/(1 + K_L C_e))$. For the solutions containing 5×10^{-4} mol L^{-1} ($\approx$100 mg L^{-1}) of Pb^{2+}, UO_2^{2+} or Th^{4+}, the amounts of PAA-Apt for removal of any of the ions from 100% to 50–0.1% were estimated to be 0.3–0.5, 0.2–0.3 and 0.5–1 mg L^{-1} for Pb^{2+}, UO_2^{2+} and Th^{4+}, respectively. Such low amounts should also be considered as an evidence for the effectiveness of the proposed adsorbent.

3.3. Adsorption thermodynamics

$1/T$ as a function of $\ln K_d$ was depicted in Fig. 4 to obtain temperature dependence of the adsorption of the studied ions. The thermodynamic parameters derived from the depictions and free

Table 2
Thermodynamic parameters for Pb^{2+}, UO_2^{2+} ve Th^{4+} adsorption onto Apt and PAA–Apt

	ΔH (kJ mol^{-1})	ΔS (J mol^{-1} K^{-1})	ΔG (kJ mol^{-1})	R^2	E_{DR} (kJ mol^{-1})
Pb^{2+}					
Apt	10.9	71	−10.3	0.868	9.2
PAA–Apt	6.4	65	−13.0	0.886	10.3
UO_2^{2+}					
Apt	4.3	56	−12.4	0.990	6.9
PAA–Apt	7.4	72	−14.0	0.996	13.0
Th^{4+}					
Apt	1.6	44	−11.5	0.980	6.9
PAA–Apt	1.4	52	−14.1	0.992	7.1

energy change (E_{DR}) derived from DR model were introduced in Table 2.

The enthalpy and entropy changes were ΔH and $\Delta S > 0$ for all ions for both Apt and PAA–Apt, i.e. the overall process was endothermic and the randomness in the solid-solution interface increased along with the adsorption process. Gibbs free enthalpy change was $\Delta G < 0$ indicating that the adsorption process was spontaneous. The ΔH and ΔG values also signified that the absorbability was in favor of Th^{4+} for both adsorbents.

$E_{DR} \cong 8$ kJ mol^{-1} has been assumed as a threshold for definition of the nature of adsorption; the physical forces such as diffusion process is effective on sorption if $E_{DR} < 8$ kJ mol^{-1}, the process is

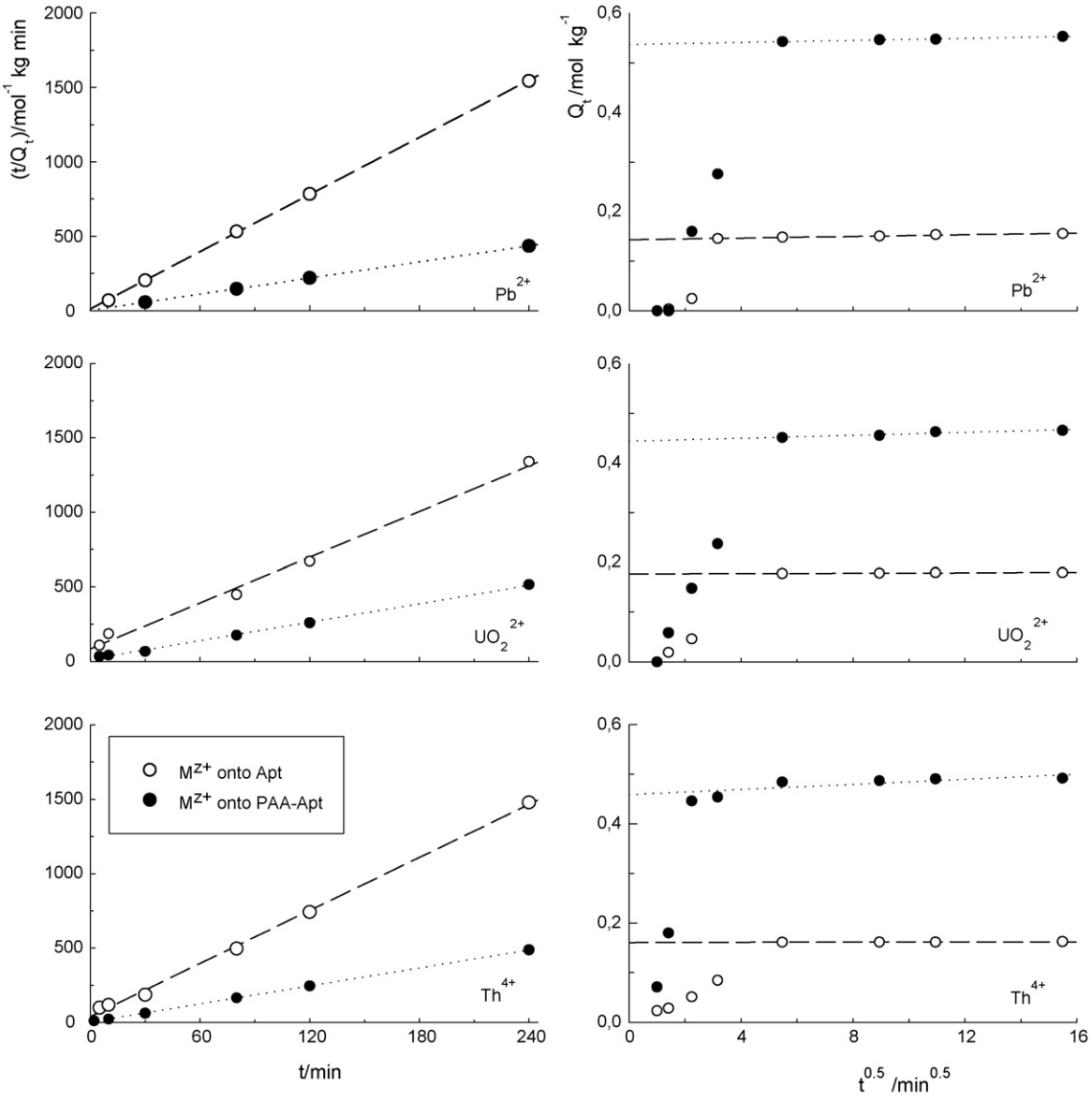

Fig. 5. Compatibility of Pb^{2+}, UO_2^{2+} and Th^{4+} adsorption kinetics for Apt and PAA–Apt to pseudo-second-order (t/Q_t vs. t) and intraparticle diffusion (Q_t vs. $t^{0.5}$) models.

Table 3
Kinetic parameters for Pb^{2+}, UO_2^{2+} and Th^{4+} adsorption onto Apt and PAA–Apt

	Pseudo-second-order kinetic					Intrapartical diffusion	
	k (mol^{-1} kg min^{-1})	Q_{Mod} (mol kg^{-1})	Q_e (mol kg^{-1})	H (mol kg^{-1} min^{-1})	R^2	$k_i \times 10^4$ (mol kg^{-1} $min^{0.5}$)	R^2
Pb^{2+}							
Apt	10.6	0.15	0.16	0.24	0.999	8.3	0.968
PAA–Apt	3.35	0.55	0.55	1.00	0.999	10.2	0.990
UO_2^{2+}							
Apt	0.24	0.21	0.18	0.01	0.965	1.8	0.798
PAA–Apt	0.16	0.47	0.53	0.03	0.979	14.8	0.911
Th^{4+}							
Apt	0.44	0.18	0.16	0.01	0.975	1.2	0.976
PAA–Apt	0.55	0.53	0.49	0.05	0.989	26.9	0.908

the ion exchange other vice [36,37]. The E_{DR} values were high or close to the threshold. Evaluation of E_{DR} and ΔG values together indicated that the sorption process is either the ion exchange or complex formation but it is chemical. The rise in E_{DR} of UO_2^{2+} for PAA–Apt in comparison to that for Apt was also an evidence for the barrier effect of PAA to UO_2^{2+} ions on reaching to the adsorptive sites on Apt.

3.4. Kinetics of adsorption

The compatibility of experimental data to the second-order kinetics and intraparticle diffusion models were evaluated with reference to the statistical significance of linearity obtained from t to t/Q_t and $t^{0.5}$ to Q_t plots (Fig. 5).

The rate controlling mechanism is chemical processes if the second-order model provides a statistically meaningful regression coefficient [31,37]. Beside this, the values of adsorbed amounts at equilibrium obtained from the model (Q_{Mod}) should also be close to that obtained from the experiment (Q_e). The results of this investigation were well compatible to the second-order model ($p < 0.01$) and provided Q_{Mod} close to Q_e values. These findings (Table 3) eventually confirmed that the nature of adsorption was concentration dependent so that the rate-controlling step is chemical sorption via complex formation and/or ion exchange.

The linear curve obtained from $t^{0.5}$ to Q_t plot should pass through the origin, if the adsorption is diffusion controlled. The plots obtained from this investigation was not provided intercepts at origin but provided a curve that could be evaluated in two linear parts; the one with a steep rise and the other with a lower slope resembling a plateau. The former defines the initial rapid uptake by the boundary layer effects whilst the latter is associated with the intraparticle diffusion taking place after the completion of external surface coverage by the former process [13]. The significant increase in both initial adsorption (H) and intraparticle diffusion (k_i) in favor of PAA–Apt for all studied ions should also be evidences for the expansion of adsorptive surfaces of Apt dispersed in PAA network enabling a faster uptake by the surface and transfer of ions towards inner active sites. Indeed, the time required for completion of the adsorption process was mainly 30 min.

3.5. Ion selectivity and reusability

The results of ion selectivity of the adsorbent in the presence of the ions with all possible combinations at equivalent concentrations (5×10^{-3} mol L^{-1}) were provided in Table 4. Both Apt and PAA–Apt had the highest affinity to Pb^{2+} in the presence of UO_2^{2+} and of both UO_2^{2+} and Th^{4+}. This can also be explained by the effects of the effective ionic charge and the parameters related to the affinity of Pb^{2+} to the adsorbents (K_L and β, see Table 1) together with the ionic strength of the medium; it appears that all were in favor of Pb^{2+}. Apt was not selective for Th^{4+} or Pb^{2+} but PAA–Apt was considerably selective for Th^{4+} in the presence of this couple, which should again be related to the effective ionic charge. The barrier effect of PAA in PAA–Apt was also obviously seen for the other possible combination, the adsorbed amounts from solutions containing UO_2^{2+} and Th^{4+} were 85 and 33% for Apt, whilst those were 43 and 55% for PAA–Apt.

The reusability feature of Apt and PAA–Apt was tested for Pb^{2+} for four regenerations in a total of five uses. The means and its ±S.E.M. of the percentage adsorption of the ion onto the adsorbents and the regeneration efficiency obtained from the four following uses after the first were $38.4 \pm 0.4\%$ and $97 \pm 1\%$ for Apt and $53.2 \pm 0.7\%$ and $98 \pm 1\%$ for PAA–Apt. The values of means were not significantly different from the values of their first use; 39.6 and 54.6% assumed to be 100% ($p < 0.05$). The IR spectra obtained before and after reuses provided no evidence signifying any changes in the structures. Storage foregoing had also no effect on the structural stability.

After emphasizing the above mentioned adsorptive features, the sorption capacity of the composite together with that of Apt for the ions of interest were compared with those extracted from literature in Table 5. The comparison obviously showed that PAA–Apt should be considered amongst the favorite adsorbents besides its cost effectiveness.

3.6. Chemical nature of adsorption

1. Investigations with Apt minerals demonstrated that they had high retaining capacity for a large numbers of cations

Table 4
Metal selectivity of Apt and PAA–Apt from solutions containing possible combinations of studied ions at equivalent concentrations (5×10^{-3} mol L^{-1})

Combinations	Adsorption (%)	
	Apt	PAA–Apt
Pb^{2+}, UO_2^{2+} and Th^{4+}		
Pb^{2+}	86[a] (42)[b]	93 (51)
UO_2^{2+}	82 (40)	40 (22)
Th^{4+}	36 (18)	49 (27)
Pb^{2+} and UO_2^{2+}		
Pb^{2+}	85 (63)	94 (67)
UO_2^{2+}	50 (37)	47 (33)
Pb^{2+} and Th^{4+}		
Pb^{2+}	39 (48)	28 (33)
Th^{4+}	42 (52)	56 (67)
UO_2^{2+} and Th^{4+}		
UO_2^{2+}	85 (72)	43 (44)
Th^{4+}	33 (28)	55 (56)

[a] As percentage of the amount of ion added to the solution.
[b] As percentage of total ion adsorption onto the adsorbent.

Table 5
Comparison of Pb^{2+}, UO_2^{2+} and Th^{4+} adsorption capacities of various adsorbents extracted from literature

Adsorbent	X (mol kg^{-1})	Reference
Pb^{2+}		
Apt and PAA–Apt	0.28; 0.81	This study
Calcined phosphate	0.41	[38]
Natural and activated phosphate	0.56; 0.75	[39]
Zirconium(IV) phosphate chemically grafted onto silica gel	0.01	[40]
Crosslinked carboxymethyl-chitosan	1.89	[41]
Chitosan granules functionalized with poly(acrylic acid)	1.42	[42]
Xanthated, phosphorylated and natural chitin	1.41; 1.20; 1.14	[43]
Chitosan (Ch) and PAA–Ch composite	0.38; 0.84	[34]
Microporous titanosilicate	1.12	[44]
Poly(ethylenimine) coated onto silica gels	0.60	[45]
Bentonite (B), zeolite (Z) and PAA-B and PAA-Z composites	0.16; 0.28; 0.18; 1.65	[23]
Carbon nanotubes	0.14	[46]
Palm kernel fiber	0.28	[47]
Poly(phenylenediamine) microparticles	0.88	[2]
Co-polymer of styrene and divinyl-benzene™	2.11	[48]
UO_2^{2+}		
Apt and PAA–Apt	1.33; 0.69	This study
Polyacrylonitryl–synthetic and natural zeolite composites	0.38; 0.37	[49]
Non-pretreated, protonated and Ca-pretreated algae	0.83; 1.19; 1.70	[50]
Chitosan-coated perlite	0.55	[51]
Chitosan (Ch) and PAA–Ch composite	0.14; 0.27	[34]
Calcined diatomite	0.40	[52]
Methacryloylamidoglutamic acid functionalized poly(2-hydroxyethyl methacrylate) beads	0.76	[53]
Poly(*N*-vinyl 2-pyrrolidone-*g*-citric acid) hydrogels	0.58	[54]
Manganese oxide coated zeolite	0.06	[55]
PAA–bentonite composite and its modification by phytic acid	0.19; 0.11	[22]
Th^{4+}		
Apt and PAA–Apt	0.41; 1.27	This study
Polyacrylonitryl–synthetic and natural zeolite composites	1.61; 1.52	[49]
Activated carbon, natural and synthetic zeolite	1.18; 0.85; 2.82	[56]
Myrica rubra and larch tannins immobilized onto collagen fibers	0.32; 0.08	[57]
Titanium phosphate	0.35	[58]
Chitosan (Ch) and PAA–Ch composite	0.39; 1.53	[34]

via three processes namely; isomorphous substitutions and diffusion, complexation reactions with functional groups of the surface, and the formation of insoluble compounds via dissolution–precipitation [5,10,14,16]. The results of this investigation suggest that the most possible mechanism is the complexation reactions, for which the increase in adsorption capacity and spontaneity as a result of the expansion of adsorptive surface due to the dispersion of Apt in PAA, and the reusability after reconditioning of the adsorbents with HCl were evidences.

2. According to Smiciklas et al. [13], the initial and final pH remains unchanged when a metal sorption occurs in solutions with initial pH in the range of 4–10 since Apt buffers aqueous solutions with reference to the following reactions:

$$\equiv PO^- + H^+ \leftrightarrow \equiv POH^0$$

$$\equiv CaOH_2^+ \leftrightarrow \equiv CaOH^0 + H^+$$

The study performed for pH dependence of adsorption for the range of 1–5 indicated that the adsorption increases with increasing pH and reached maximum at around pH 4. The low adsorption at pH 1–3 should be associated with the repulsive forces between the metal ions and positively charged (protonated) adsorptive surface, after which the buffering mechanism dominates at pH 4 and its beyond. However, the range of pH values obtained from the studies for adsorption isotherms were always 3–5 at initial and reached to constancy providing a range of 4–5 immediately after adsorbent/solution contact and remained unchanged. By considering that the major species of the studied ions in solutions with these pH ranges are Pb^{2+}, UO_2^{2+} and Th^{4+} [5,59,60] and ≡POH is the predominant form for the surface sorption on the based of the models postulated by Simon et al. [11] and Wu et al. [61] for Pb^{2+} and UO_2^{2+}, the chemical nature of adsorption should consequently be generalized for also Th^{4+} and given in the following reactions:

$$\equiv OH + M^{Z+} \leftrightarrow \equiv O\text{–}M^{(Z+)-1} + H^+$$

$$\equiv O_3P\text{–}OH^+ + M^{Z+} \leftrightarrow \equiv O_3P\text{–}O\text{–}M^{(Z+)-1} + H^+$$

4. Conclusion

In this study, the preparation and characterization of PAA–Apt micro-composite and its comparative adsorptive features with bare Apt were investigated for Pb^{2+}, UO_2^{2+} and Th^{4+}.

The FT-IR, XRD and SEM analysis showed that PAA–Apt had a hybrid composition of PAA and Apt resembling colloidal dispersion of one solid phase (Apt) in another.

Experimentally obtained isotherms were well compatible to Langmuir, Freundlich and DR models, from which the derived parameters were confirmed each other. Adsorption capacity of Apt in PAA was higher than that of bare Apt for $Pb^{2+}$and Th^{4+}, whilst it was lower for UO_2^{2+}. The spontaneity of adsorption increased for both $Pb^{2+}$and UO_2^{2+} but unchanged for Th^{4+}.

The values of enthalpy and entropy changes were positive for all studied ions for both Apt and PAA–Apt. The negative free enthalpy change was evidence for the spontaneity of adsorption. The compatibility of adsorption kinetics to the second order and intraparticle diffusion models implied that the rate controlling step

was concentration dependent, i.e. the sorption process was chemical that followed by intraparticle diffusion. The chemical nature of the adsorption for all studied ions was consistent with both thermodynamic parameters and the free energy changed obtained from DR model.

Both Apt and PAA–Apt had the highest affinity to Pb^{2+} in the presence of the other two ions. The regeneration tests for Apt and PAA–Apt for Pb^{2+} for five uses proved that the adsorbents can be reused after complete recovery of the loaded ion.

In consequence, the use of Apt in the composite form significantly enhanced the adsorptive features of Apt.

Acknowledgement

This work was supported by The Research Fund of Cumhuriyet University to which the authors are grateful.

References

[1] X.G. Li, R. Liu, M.R. Huang, Facile synthesis and highly reactive silver ion adsorption of novel microparticles of sulfodiphenylamine and diaminonaphthalene copolymers, Chem. Mater. 17 (2005) 5411–5419.
[2] M.R. Huang, Q.Y. Peng, X.G. Li, Rapid and Effective Adsorption of Lead Ions on Fine Poly(phenylenediamine) Microparticles, Chem. Eur. J. 12 (2006) 4341–4350.
[3] M.R. Huang, H.J. Lu, X.G. Li, Efficient multicyclic sorption and desorption of lead ions on facilely prepared poly(*m*-phenylenediamine) particles with extremely strong chemoresistance, J. Colloid Interface Sci. 313 (2007) 72–79.
[4] S.J.T. Pollard, G.D. Fowlerr, C.J. Sollars, R. Perry, Low-cost adsorbents for waste and wastewater treatment: a review, Sci. Tot. Environ. 116 (1992) 31–52.
[5] A. Krestou, A. Xenidis, D. Panias, Mechanism of aqueous uranium (VI) uptake by hydroxyapatite, Miner. Eng. 17 (2004) 373–381.
[6] E. Mavropoulos, C.C.N. Rocha, C.J. Moreira, C.L. Bertolino, M.A. Rossi, Pb^{2+}, Cu^{2+} and Cd^{2+} ions uptake by Brazilian phosphate rocks, J. Braz. Chem. Soc. 16 (2005) 62–68.
[7] E. Deydier, R. Guilet, P. Sharrock, Beneficial use of meat and bone meal combustion residue: an efficient low cost material to remove lead from aqueous effluent, J. Hazard. Mater. B101 (2003) 55–64.
[8] I. Smiciklas, A. Onjia, S. Raicevic, Experimental design approach in the synthesis of hydroxyapatite by neutralization method, Sep. Purif. Technol. 44 (2005) 97–102.
[9] M. Federoff, J. Jeanjean, J.C. Rouchaud, L. Mazerolles, Sorption kinetics and diffusion of cadmium in calcium hydroxyapatites, Solid State Sci. 1 (1999) 71–84.
[10] S. McGrellis, J.-N. Serafini, J. Jeanjean, J.-L. Pastol, M. Federoff, Influence of the sorption protocol on the uptake of cadmium ions in calcium hydroxyapatite, Sep. Purif. Technol. 24 (2001) 129–138.
[11] F.G. Simon, V. Biermann, C. Segebade, M. Hedrich, Behavior of uranium in hydroxyapatite-bearing permeable reactive barriers: investigation using ^{237}U as a radioindicator, Sci. Total. Environ. 326 (2004) 249–256.
[12] R.C. Moore, M. Gasser, N. Awwad, C.K. Holt, M.F. Salas, A. Hasan, M. Hasan, H. Zhao, C.A. Sanchez, Sorption of plutonium(VI) by hydroxyapatite, J. Radioanal. Nucl. Chem. 263 (2005) 97–101.
[13] I. Smiciklas, S. Dimovic, I. Plecas, M. Mitric, Removal of Co^{2+} from aqueous solutions by hydroxyapatite, Water Res. 40 (2006) 2267–2274.
[14] S. Sugiyama, H. Matsumoto, H. Hayashi, J.B. Moffat, Sorption and ion-exchange properties of barium hydroxyapatite with divalent cations, Colloid Surf. 169 (2000) 17–26.
[15] S. Sugiyama, H. Matsumoto, T. Ichii, H. Hayashi, Y. Hiraga, N. Shigemoto, Enhancement of lead-barium exchangeability of barium hydroxyapatite, J. Colloid Interface Sci. 238 (2001) 183–187.
[16] J. Perrone, B. Fourest, E. Giffaut, Sorption of nickel on carbonate fluoroapatites, J. Colloid Interface Sci. 239 (2001) 303–313.
[17] M. Sarioglu, Ü.A. Atay, Y. Cebeci, Removal of copper from aqueous solutions by phosphate rock, Desalination 181 (2005) 303–311.
[18] J. Andersson, S. Areva, B. Spliethoff, M. Linden, Sol–gel synthesis of a multifunctional, hierarchically porous silica/apatite composite, Biomaterials 26 (2005) 6827–6835.
[19] L.E. Hammari, A. Laghzizil, A. Saoiabi, P. Barboux, M. Meyer, Chemical modification of porous calcium hydroxyapatite surfaces by grafting phenylphosphonic and phenylphosphite acids, Colloid Surf. 289 (2006) 84–88.
[20] J. Pena, I. Izguierdo-Barba, A.M. Garcia, M. Vallet-Regi, Room temparature synthesis of chitosan/apatite powders and coatings, J. Eur. Ceram. Soc. 26 (2006) 3631–3638.
[21] L.Q. Li, Z.Q. Chen, B.W. Darvell, Q. Zeng, G. Li, G.-M. Ou, M.-Y. Wu, Biomimetic synthesis of the composites of hydroxyapatite and chitosan-phosphorylated chitosan polelectrolyte complex, Mater. Lett. 60 (2006) 3536–3553.
[22] U. Ulusoy, S. Şimşek, Ö. Ceyhan, Investigations for modification of polyacrylamide-bentonite by phytic acid and its usability in Fe^{3+}, Zn^{2+} and UO_2^{2+} Adsorption, Adsorption 9 (2003) 165–175.
[23] U. Ulusoy, S. Şimsek, Lead removal by polyacrylamide-bentonite and zeolite composites: Effect of phytic acid immobilization, J. Hazard. Mater. 127 (2005) 163–171.
[24] M. Alexandre, P. Dubois, Polymer-layered silicate nanocomposites: Preparation, properties and uses of a new class of materials, Mat. Sci. Eng. 28 (2000) 1–63.
[25] J.J. Lin, Y.M. Chen, Amphiphilic properties of poly(oxyalkylene)amine-intercalated smectite aluminosilicates, Langmuir 20 (2004) 4261–4264.
[26] J. Domb, E.G. Cravalho, R. Langer, The synthesis of poly(hydroxamic acid) from poly(acrylamide), J. Polym. Sci. A: Poly. Chem. 26 (1988) 2623–2630.
[27] H. Rohwer, N. Rheeder, E. Hosten, Interactions of uranium and thorium with arsenazo III in an aqueous medium, Anal. Chim. Acta 341 (1997) (1997) 263–268.
[28] M.H. Khan, A. Ali, N.N. Khan, Spectrophotometric determination of thorium with disodium salt of Arsenazo-III in perchloric acid, J. Radioanal. Nucl. Chem. 250 (2001) 353–357.
[29] H. Omichi, A. Katakai, T. Sugo, J. Okamoto, A new type of amidoxime-group-containing adsorbent for the recovery of uranium from seawater, 3 recycle use of adsorbent, Sep. Sci. Technol. 21 (1986) 563–574.
[30] Y.S. Ho, G. McKay, Pseudo-second order model for sorption processes, Proc. Biochem. 34 (1999) 451–465.
[31] L. Yun, S. Xing, C. Haidong, Z. Huixian, G. Shixiang, Adsorption of copper and lead in aqueous solution onto bentonite modified by 4′-methylbenzo-15-crown-5, J. Hazard. Mater. 137 (2006) 1149–1155.
[32] S. Sun, A. Wang, Adsorption kinetics of Cu (II) ions using N,O-carboxymethyl-chitosan, J. Hazard. Mater. 131 (2006) 103–111.
[33] M. Randhawa, I. Gartner, C. Becker, J. Student, M. Chai, A. Mueller, Imprinted polymers for water purification, J. Appl. Polym. Sci. 106 (2007) 3321–3326.
[34] R. Akkaya, U. Ulusoy, Adsorptive features of chitosan entrapped in polyacrylamide hydrogel for Pb^{2+}, UO_2^{2+}, and Th^{4+}, J. Hazard. Mater. 151 (2008) 380–388.
[35] M. Doğan, M. Alkan, Removal of methyl violet from aqueous solution by perlite, J. Colloid Interface Sci. 267 (2003) 32–41.
[36] B.S. Krishna, D.S.R. Murty, B.S. Jai Prakash, Thermodynamics of chromium(VI) anionic species sorption onto surfactant-modified montmorillonite clay, J. Colloid Interface Sci. 229 (2000) 230–236.
[37] A.R. Cestari, V.F. Eunice, C.R.S. Mottos, Thermodynamics of the Cu (II) adsorption on thin vanillin-modified chitosan membranes, J. Chem. Thermodyn. 38 (2006) 1092–1099.
[38] A. Aklil, M. Mouflihb, S. Sebti, Removal of heavy metal ions from water by using calcined phosphate as a new adsorbent, J. Hazard. Mater. A 112 (2004) 183–190.
[39] M. Mouflih, A. Aklil, S. Sebti, Removal of lead from aqueous solutions by activated phosphate, J. Hazard. Mater. B 119 (2005) 183–188.
[40] N. Nagata, L.T. Kubota, M.I.M.S. Bueno, P.G. Peralta-Zamora, Adsorption parameters of Cd(II), Pb(II), and Hg(II) on zirconium(IV) phosphate chemically grafted onto silica gel surface, J. Colloid Interface Sci. 200 (1998) 121–125.
[41] S. Sun, L. Wang, A. Wang, Adsorption properties of crosslinked carboxymethyl-chitosan resin with Pb(II) as template ions, J. Hazard. Mater. B 136 (2006) 930–937.
[42] N. Li, R. Bai, Highly enhanced adsorption of lead ions on chitosan granules functionalized with poly(acrylic acid), Ind. Eng. Chem. Res. 45 (2006) 7897–7904.
[43] S.H. Kim, H. Song, G.M. Nisola, J. Ahn, M.M. Galera, C.H. Lee, W.J. Chung, Adsorption of lead(II) ions using surface-modified chitins, J. Ind. Eng. Chem. 12 (2006) 469–475.
[44] G.X.S. Zhao, J.L. Lee, P.A. Chia, Unusual adsorption properties of microporous titanosilicate ETS-10 toward heavy metal lead, Langmuir 19 (2003) 1977–1979.
[45] M.L. Delacour, E. Gaılliez, M. Bacquet, M. Morcellet, Poly(ethylenimine) coated onto silica gels: adsorption capacity toward lead and mercury, J. Appl. Polym. Sci. 73 (1999) 899–906.
[46] Y.-H. Li, S. Wang, J. Wei, X. Zhang, C. Xu, Z. Luan, D. Wu, B. Wei, Lead adsorption on carbon nanotubes, Chem. Phys. Lett. 357 (2002) 263–266.
[47] Y.S. Ho, A.E. Ofomaja, Pseudo-second-order model for lead ion sorption from aqueous solutions onto palm kernel fiber, J. Hazard. Mater. B 129 (2006) 137–142.
[48] M.H. Entezari, T.R. Bastami, Sono-sorption as a new method for the removal of lead ion from aqueous solution, J. Hazard. Mater. B 137 (2006) 959–964.
[49] S. Akyil, M. Eral, Preparation of composite adsorbents and their characteristics, J. Radioanal. Nucl. Chem. 266 (2005) 89–93.
[50] M.H. Khani, A.R. Keshtkar, B. Meysami, M.F. Zarea, R. Jalali, Biosorption of uranium from aqueous solutions by nonliving biomass of marine algae cystoseira indica, J. Electron. Biotechnol. 9 (2006) 100–106.
[51] S. Hasan, T.K. Ghosh, M.A. Prelas, D.S. Viswanath, V.M. Boddu, Adsorption of uranium on a novel bioadsorbent-chitosan-coated perlite, Nucl. Technol. 159 (2007) 59–71.
[52] Ş.O. Aytaş, S. Akyil, M.A. Aslani, U. Aytekin, Removal of uranium from aqueous solutions by diatomite (Kieselguhr), J. Radioanal. Nucl. Chem. 240 (1999) 973–976.
[53] A. Denizli, R. Say, B. Garipcan, S. Patir, Methacryloylamidoglutamic acid functionalized poly(2-hydroxyethyl methacrylate) beads for UO_2^{2+} removal, React. Funct. Polym. 58 (2004) 123–130.
[54] T. Çaykara, S. Ören, Ö. Kantoglu, O. Güven, The effect of gel composition on the uranyl ions adsorption capacity of poly(*N*-vinyl 2-pyrrolidone-g-citric

acid) hydrogels prepared by gamma rays, J. Appl. Polym. Sci. 77 (2000) 1037–1043.
[55] R. Han, W. Zou, Y. Wang, L. Zhu, Removal of uranium (VI) from aqueous solutions by manganese oxide coated zeolite: discussion of adsorption isotherms and pH effect, J. Environ. Radiat. 93 (2007) 127–143.
[56] M. Metaxas, V. Kasselouri-Rigopoulou, P. Galiatsatou, C. Konstantopoulou, D. Oikonomou, Thorium removal by different adsorbents, J. Hazard. Mater. B 97 (2003) 71–82.
[57] X. Liao, L. Li, B. Shi, Adsorption recovery of thorium(IV) by Myrica rubra tanin and larch tannin immobilized onto collagen fibres, J. Radioanal. Nucl. Chem. 260 (2004) 619–625.
[58] K. Maheria, U. Chudasama, Studies on kinetics, thermodynamics and sorption characteristics of an inorganic ion exchanger-titanium phosphate towards Pb(II), Bi(III) and Th(IV), J. Indian Inst. Sci. 86 (2006) 515–525.
[59] Z.X. Sun, R.O. Sköld, A Multi-parameter titration method for the determination of formation pH for metal hydroxides, Miner. Eng. 14 (2001) 1429–1443.
[60] R.J. Murphy, J.J. Lenhart, B.D. Honeyman, The sorption of thorium(IV) and uranium(VI) to hematite in the presence of natural organic matter, Colloid Surf. 157 (1999) 47–62.
[61] L. Wu, W. Forling, P.W. Schindler, Surface complexation of calcium minerals in aqueous solution, 1. Surface protonation at fluorapatite-water interfaces, J. Colloid Interface Sci. 147 (1991) 178–185.